Ceria-Incorporated Activated Carbon Composite as Electrode Material for Capacitive Deionization

Nasser Zouli

Department of Chemical Engineering, Faculty of Engineering, Jazan University, Jazan, Saudi Arabia.
E-mail: nizouli@jazanu.edu.sa

Capacitive deionization (CDI) has attracted attention as a low-energy technology for electrochemical water desalination. Given the low cost and availability of activated carbon (AC), it has been identified as a promising electrode material for CDI, but it suffers from AC low specific capacitance and hydrophobic characteristics. In this research, ceria (CeO_2) nanoparticles were incorporated into AC and applied in the hydrothermal treatment process. CeO_2 has been shown to play a key function in improving the electrochemical and electrosorption activity of AC, thereby resolving the capacitance and hydrophobicity limitations. A single-batch mode CDI cell was used to test desalination performance. The results showed that the best-performing AC electrode material was 5 wt.% CeO_2@AC, which achieved a specific capacitance of 262 Fg^{-1} and electrosorption capacity of 8.9 mg g^{-1} under the conditions of 100 μS cm^{-2} NaCl solution at 1.4 V. This material is recommended as an attractive candidate for water desalination in CDI applications.

1. INTRODUCTION

Water demand has increased substantially worldwide due to population growth and new technological and agricultural uses for water, but scarcity remains one of the most urgent and impactful problems of the twenty-first century [1, 2]. One of the most sustainable solutions for the emerging global water crisis involves the desalination of sea or brackish water [3]. Although water desalination technologies exist, including reverse osmosis, multi-stage water distillation, ion exchange, and large-scale electrolysis, these solutions typically have a sizeable energy demand, high costs, and complex maintenance routines [4].

Alongside the global water crisis and the poor sustainability performance of existing water desalination solutions, trends in energy conservation and environmental protection have heightened the need to find clean, affordable, and safe water desalination technologies. Capacitive deionization (CDI)

is a novel desalination technology characterized by limited energy consumption, straightforward maintenance and operation, and an eco-friendly performance [5, 6]. For this reason, CDI has attracted the attention of the research community as a low-energy technology for electrochemical water desalination.

CDI systems consist of a compact, modifiable structure that enables the selective removal of soluble ions in water [5, 7]. In CDI, saline water flows between a pair of electrodes that are connected to a power supply. After switching on the power supply, an electrostatic is formed between the electrodes and the ions in the solution; at the same time, the solution's cations move toward the negative electrode, whereas the anions move toward the positive electrode, thereby forming the electrode double layer (EDL) [6, 8, 9]. This step is known as ion removal or the adsorption step. The subsequent step, which is referred to as discharging or desorption, occurs when the electrodes are reversed or the power supply is deactivated; in this step, the adsorbed ions are desorbed and transferred to the bulk solution.

CDI performance is influenced by various factors, the most significant among which are the choice of electrode material and its electrochemical properties, which highlights the importance of making a careful decision [6, 10]. The optimal electrode material has a high specific capacitance, large surface area, low polarization effect, high adsorption capacity, good wettability, high chemical stability, high conductivity, rapid response to ion insertion/de-interference, good commercial opportunities, straightforward manufacturing, and low cost [9, 11-13]. In view of this, carbonaceous materials are the ideal candidates for CDI because they typically have many of these properties.

Diverse carbon materials have been employed as electrode materials in CDI, including porous carbon, activated carbon, carbon nanotubes, carbon nanofibers, and graphene. Given the distinctive properties of activated carbon (AC), particularly its low cost, availability, favorable pore-size distribution, high electrical conductivity, and large surface area (1000–2000 m^2g^{-1}), it is the best candidate electrode material from all available carbon materials for CDI [6, 10, 11, 14-20]. Additionally, since the outer surface of AC is marked by holes, cracks, and crevices, the specific surface area is considerable, which offers increased opportunities for ion entrance during CDI [21].

Despite its advantages, the value of AC as an electrode material in CDI is limited by properties such as low wettability, poor physicochemical stability, and low specific capacitance [22]. One way to resolve these limitations is to form carbonaceous composites with metal oxide [23, 24]. For these materials, metal oxide could improve the wettability, surface chemistry, charge nature, and electrochemical properties of carbon material, which is attributable to the synergistic effects with carbon. In CDI applications, various metal oxides have been tested as carbon-composite electrode materials, including TiO_2, ZrO_2, NiO, MnO_2, and SiO_2.

In the research undertaken by Wouters et al. [25], a composite material consisting of AC and TiO_2 nanoparticles (NPs) was tested as an electrode material in CDI. Under 1.2 V and 292 mg/L salt solution, the composite displayed favorable specific capacitance (380 F/g) and electrosorption capacity (17.7 mg/g). In another study, Yumak et al. [26] developed MnO_2 and NiO on AC that was prepared using a hydrothermal process. The researchers recorded a significant improvement in specific capacitance of 50% with the incorporation of NiO into AC, as well as a 150% increase in the case of MnO_2. The favorable electrochemical properties of the materials were attributed to the oxygenated functional groups available on the AC, as well as the presence of metal oxides.

Ceria (CeO_2) has been identified as a potentially valuable metal oxide for enhancing AC's performance in CDI, which is due to its good chemical stability and electrochemical conductivity, eco-friendly properties, and cost-effectiveness [27-30]. In addition, the oxidation of the state of Ce between Ce(III) and Ce(IV) facilitates rapid electron transport [31, 32]. In the literature, the creation of CeO_2-AC composite materials has been investigated as a way to improve the electrode material in CDI, particularly the limitation of the low conductivity of CeO_2. For example, Aravindan et al. [33] tested the performance of different compositions of CeO_2 (in this case, 0, 5, 10, and 15 wt.%)-AC-based composite materials prepared using simple mechanical mixing. The specific capacitance of the sample CeO_2 (10 wt.%)/AC composite electrode in the supercapacitor was 162 F/g, which exceeded the pristine AC (140 F/g) at 2 A/g and 3500 W Kg^{-1} power density at 18 $mAcm^{-2}$.

In another study involving CeO_2, Li et al. [31] reported an improvement in the electrochemical properties of graphene oxide after incorporating CeO_2. The specific capacitance of the proposed material (282 F/g), when used as an electrode material in the supercapacitor, was higher than rGO (189 F/g) at 2 A/g. The research of Ayman et al. [11] showed similar results, where CeO_2/graphene nanoflake (GNF) composites for CDI electrode displayed a higher specific capacitance (452.26 F/g) than GNFs (47.01 F/g) at 5 mVs^{-1} and higher electrosorption capacity of 7.2 mg g^{-1} than GNFs (1.2 mg g^{-1}) at 1.4 and 48 mg/L NaCL.

No prior study, to the best of our knowledge, has investigated the use of CeO_2@AC composite for water desalination. Nevertheless, a significant opportunity exists because AC is relatively easy to produce compared to alternative carbon materials. Therefore, in this study, a composite electrode material for CDI with enhanced wettability through the formation of hydrophilic groups is prepared using a hydrothermal process in high-strength alkaline solution. Analysis of the fabricated electrode according to this study's methodology involves the use of physiochemical standard techniques, while a three-electrode system is applied to examine electrochemical properties The electrode composite material is evaluated in a CDI cell to offer insights into NaCl desalination performance.

2. MATERIALS AND METHODS

2.1 Materials

For the experiment, pharma-grade activated charcoal (acid wash, LOBACheme) and cerium oxide (Loba Chemie, 99.5%, Mumbai, India) were used. Polyvinylidene fluoride (PVDF, Mw = 35000 kg mol^{-1}), potassium hydroxide (KOH, 99.99%), sodium chloride (NaCl, 99.99%), and dimethylformamide (DMF) were purchased from Sigma–Aldrich. No prior treatment was applied to the chemicals.

2.2 Preparation of CeO_2-AC composite

CeO_2 in different weight ratios (5 wt.% and 10 wt.%) and AC were combined separately with 100 mL of 5 M KOH. The mixtures were magnetically stirred for 1 h, after which they were ultra-

sonicated for 1 h. The sonicated mixtures were exposed to microwave irradiation for 50 s. In turn, the mixtures were transferred into a Teflon crucible and placed in a stainless-steel autoclave hydrothermal reactor. The reactors were heated in a muffle furnace (Thermo Fisher Scientific, 1400 °C, USA) at a temperature of 130 °C for 24 h, after which they cooled down naturally. Using distilled water, the black residues in the filter papers were washed until the pH of the filtrate was 7. The final products were dried overnight at 80 °C.

2.3 Characterization

A scanning electron microscope (JEOL, JSM-5900, Japan) was used to examine the surface morphology of the CeO_2@AC composite electrodes, while an X-ray diffractometer (Bruker Co., D8 Discover, USA) from 10° to 90° was applied to verify the crystallinity phases of the CeO_2@AC composite electrode. Moreover, the Raman spectra of AC and CeO_2@AC composite electrodes were operated through a Raman microscope (Senterra–Brucker, Germany), with its wavelength adjusted to 532 nm. Using a potentiostat (Metrohm Autolab, Netherlands), cyclic voltammetry (CV) and electrochemical impedance spectroscopy (EIS) were applied to investigate the electrochemical properties of the CeO_2@AC composite electrodes.

2.4 Electrochemical characteristics of AC and CeO_2-AC composite electrode materials

A three-electrode system was used for electrochemical CV analyses. In this study's experimental setup, Pt rode, Ag/AgCl/ (3 M KCl), and CeO_2-AC composite were attached to a glassy carbon electrode (GCE) as counter, reference, and working electrodes, respectively. Two mg of CeO_2-AC composite was added to 420 μL isopropanol and 20 μL Nafion solution and sonicated for 30 min. Following this, 15 μL sonicated solution was deposited on the GCE and dried at 80 °C for 10 min. For each electrode (AC, 5 wt.% CeO_2@AC composite, and 10 wt.% CeO_2@AC composite), the CV was determined using 1 M of NaCl aqueous solution, various scan rates, and a potential window ranging from −0.4 to 0.6 V. Additionally, a frequency response analyzer (FRA) was used for EIS in the same cell. For the alternating voltage, the amplitude was 5 mV, and it had a frequency range ranging from 10^{-2} to 10 KHz. For AC and 5 wt.% CeO_2@AC composite electrodes, the achievement of the chronopotentiostatic charge–discharge (PCDs) took place at differing applied potentials. In addition, regarding the chronogalvanostatic charge–discharge (GCD) test that was undertaken for the 5 wt.% CeO_2-AC composite electrode, this was applied at 1, 3, 5, 7, and 9 A/g.

2.5 Electrosorptive capacity measurement

Magnetic mixing took place overnight for several drops of DMF, 85 wt.% of each electrode material (AC, 5 wt.% CeO_2@AC composite, and 10 wt.% CeO_2@AC composite), and 15 wt.% PVDF. Sonication of the resulting pastes was undertaken for 1 h to achieve homogeneity, after which the pastes were coated on the carbon sheets (10×10 cm^2). The coated carbon sheets were transferred onto a drying

oven and left overnight at 80 °C. Using a peristaltic pump, an aqueous NaCl solution with an initial conductivity of ~100 μS cm^{-2} was pumped into the CDI cell at a flow rate of 10 mL/min. The electrosorption capacity of the prepared electrode materials was determined at different applied potentials (1, 1.2, and 1.4 V) using a DC power supply. An ion conductive meter (Hanna Instruments, HI-2300) was used to measure the change in the solution conductivity of the effluent. The following equation was used to evaluate the electrode electrosorption capacity (q, mg g^{-1}) at the three applied potentials:

$$q = \frac{(C_0 - C)V}{m}, \qquad (1)$$

where V (L) refers to the NaCl solution's total volume and m (g) is the total mass of the working electrodes.

3. RESULTS AND DISCUSSION

3.1 Morphology and architecture

A rock-like shape with a heterogeneous, irregular surface morphology is visible in the SEM image of pristine AC (Fig. 1A). By contrast, Fig. 2B shows the morphology of the 5 wt.% CeO$_2$@AC. Regarding the CeO$_2$ NPs, they were deposited on the AC surface and dispersed without aggregation to avoid obstructing the pores.
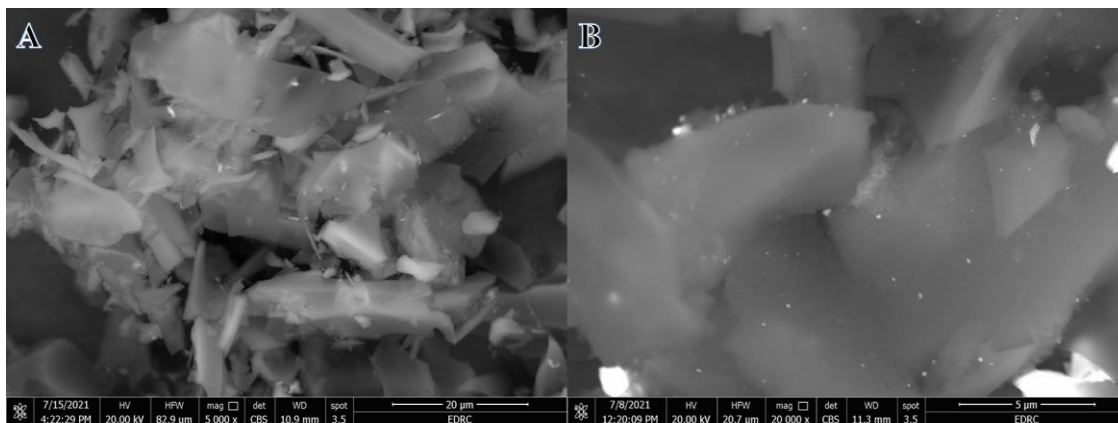
Figure 1. SEM images of pristine AC (A) and 5 wt.% CeO2@AC (B).

Fig. 2 shows the XRD analysis of pristine AC and 5 wt.% CeO$_2$@AC. AC revealed two broad peaks positioned at 2Ө values of 24.3° and 43.1°, which are consistent with the (002) and (100) crystal planes of graphite, respectively (JCPDS card no. 41-1487). A notable implication of these broad diffraction peaks is the disordered amorphous structure of the AC. Fig. 2B shows the formation of the cubic fluorite structural morphology of CeO$_2$ (JCDPs card no. 34-0394). In accordance with this, the proposed preparation process may be an effective way to fabricate CeO$_2$-decorated AC. It is noteworthy that the alkaline hydrothermal process has previously been investigated as an effective technique for the

fabrication of graphene/metal carbides and graphene/metal oxide [6, 10, 11, 34]. Regarding Raman spectroscopy, this tool can be applied to gather structural data about molecular vibrations or the rotational energy of a material. Also, Raman spectroscopy is frequently applied to provide an account of the structure of carbonaceous materials, as well as oxide materials, characterized by lattice disorder [35].
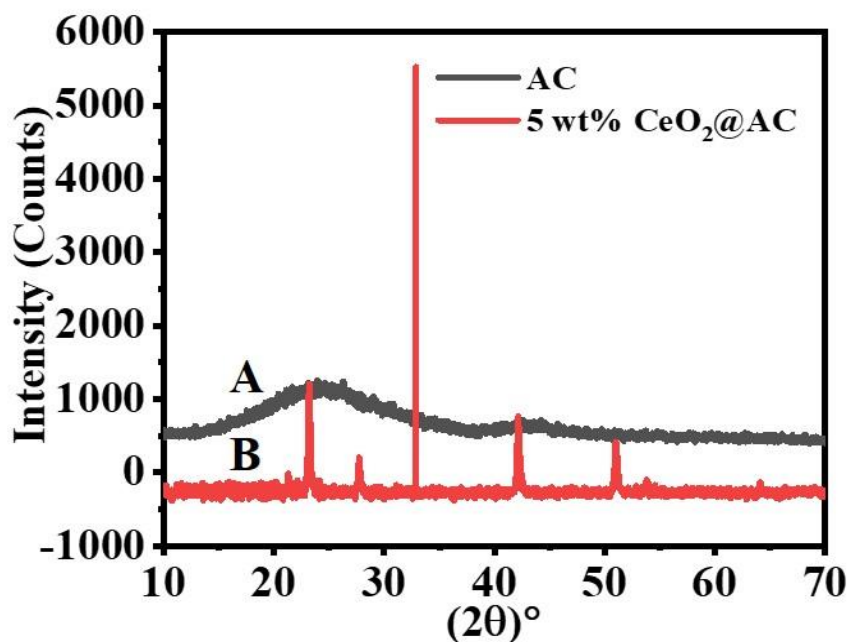
Figure 2. XRD patterns of pristine AC and 5wt% CeO_2@AC.
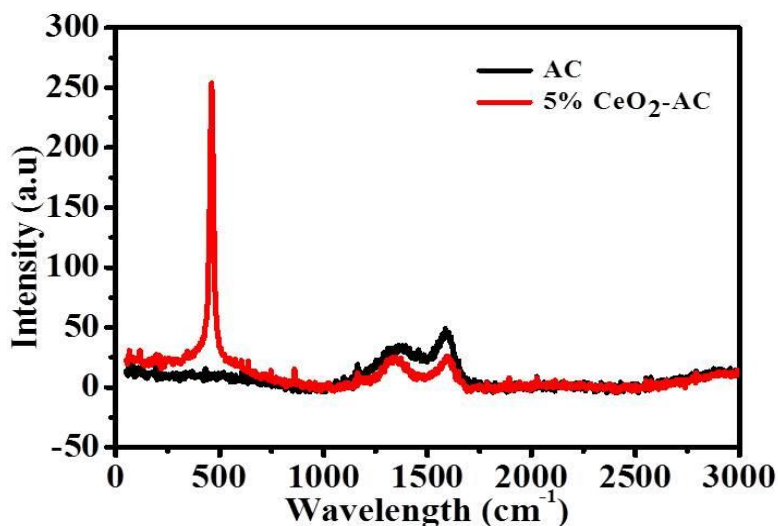
Figure 3. Raman spectra of pristine AC and AC/5wt% CeO_2.

Fig. 3 shows the Raman spectra of pristine AC and 5 wt.% CeO_2@AC. Two spectrum peaks appeared at 1350 and 1595 cm^{-1}, which are denoted as the D-band and G-band, respectively [35]. These peaks are typically found in the spectra of carbon materials. Another peak appeared for 5 wt.%

CeO_2@AC at 463 cm^{-1}, which is attributable to the F2g mode for CeO_2 with fluorite structure [36]. In the case of this particular vibrational mode, it is classified as a symmetric vibration of eight oxygen atoms around each CeO_2 cation [36].

3.2. Electrochemical characterizations

The measurement of the electrochemical performance of the two electrode materials, AC and AC@CeO_2 (5% and 10%), took place based on CV, EIS, GCD, and PCD. The CV profile of AC and CeO_2@AC with a sweep rate of 10 mV/s in a 1 M NaCl aqueous solution, along with the potential window ranging from −0.4 to 0.6 V, is shown in Fig. 4A. Every sample was characterized by a rectangular CV profile without any faradic reactions in the applied potential range. This is suggestive of the optimal capacitive behavior of the electrode materials, which is attributable to EDL formation [37]. The formation of EDL was a result of Coulombic interaction rather than redox reactions [38]. Furthermore, as shown by the symmetrical rectangular CV shapes of the electrode materials, it was possible for the solution's ions to be electro-adsorbed on the electrode materials in an efficient and rapid way [39]. EDL formation, along with the rise in the current density of the as-prepared composite electrode materials, was marked by optimal and quickly reversible capacitor behavior [40]. In most cases, the incorporation of CeO_2 improved AC's electrochemical properties. As indicated in the figure, the 5 wt.% CeO_2@AC composite electrode significantly outperformed AC and 10 wt.% CeO_2@AC in terms of the largest integrated area and current density.
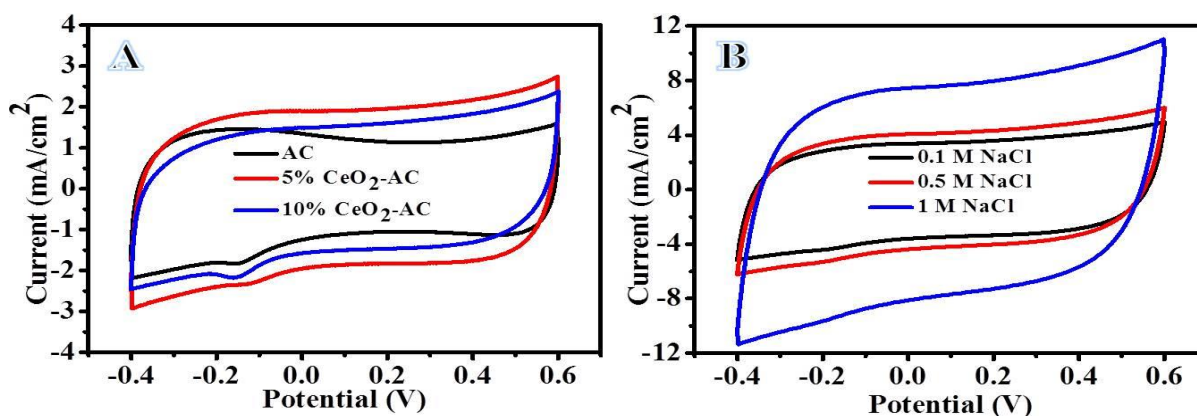
Figure 4. Cyclic voltammograms of AC, 5 wt.% CeO_2@AC, and 10 wt.% CeO_2@AC in 1 M NaCl solution at 10 mV s^{-1} (A). Effect of salt concentration on 5 wt.% CeO_2@AC composite electrode at 50 mV s^{-1}(B).

This is reflective of the material's high contact area, high capacitance, low interfacial resistance, and favorable electrochemical performance [56]. Nevertheless, as a result of the incorporation of CeO_2 above 5 wt.%, this was associated with a negative impact on electrochemical behavior, which could be attributable to the obstruction of the AC pores [11]. Fig. 4B presents the CV curves for the 5 wt.%

CeO$_2$@AC composite electrode material at different NaCl concentrations (0.1, 0.5, and 1 M) and a scan rate of 50 mV s^{-1}. Higher salt concentration was associated with an improvement in electrochemical performance, indicating high electrosorption capacity even in hard saturation. Moreover, the area of CV grew with higher NaCl concentration, which suggests high specific capacitance and the electrosorption of ions in the EDL region [22]. Therefore, as a composite electrode material, these experiments indicate that 5 wt.% CeO$_2$@AC displayed good electrosorption.

The CV performance of 5 wt.% CeO$_2$@AC at different scan rates (5, 10, 25, 50, 75, and 100) mV s^{-1}) is shown in Fig. 5A. The experimental condition was a 1 M NaCl aqueous solution with the potential window ranging from −0.4 to 0.6 V. In this case, the CV plots moved from rectangular shapes to oval shapes with the scan rate rising from 5 mV s^{-1} to 100 mV s^{-1} in 1 M NaCl solution. This may be due to the fact that at high scan rates, salt solutions have inherent resistivity with respect to ion movement, which negatively influences EDL formation [41]. Noteworthily, reducing the scan rate has a positive impact on ion adsorption into the electrode and enhances electrode reversibility [42, 43]. Furthermore, when the scan rate is low, it is possible for ions to move from the bulk solution to the electrode surface with sufficient time; by contrast, if the scan rate is high, there is insufficient time to transport ions to the electrode.
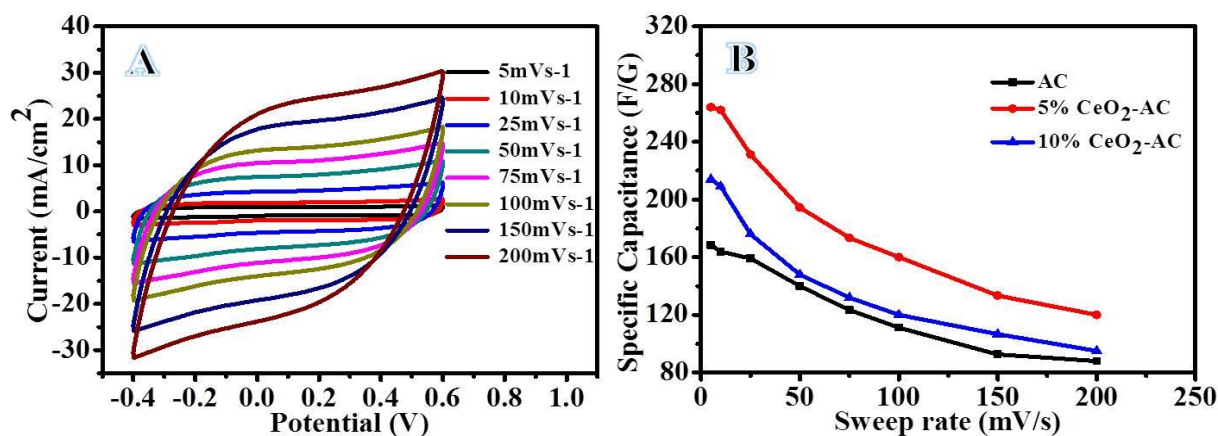
Figure 5. Cyclic voltammograms of 5 wt.% CeO$_2$@AC in 1.0 M NaCl solution at different scan rates (5, 10, 25, 50, 75 and 100 mV s^{-1}) (A). Corresponding specific capacitance values of AC, 5 wt.% CeO$_2$@AC, and 5 wt.% CeO$_2$@AC electrode materials, which vary as a function of scan rate in (B).

It has been empirically established that the property of specific capacitance (C$_s$, Fg^{-1}) is a fundamental factor to consider when assessing an electrode material's CDI. For a fabricated electrode, it is possible to estimate the C$_s$ values by integrating the whole CVs at different scan rates. This yields an average value, as shown in the following equation [6, 10, 11]:

$$Cs = \frac{\int i dV}{2v\Delta V m} \qquad (2)$$

In this equation, C_s denotes the specific capacitance (F g^{-1}), i represents the current (A), V is the potential (V), m is the mass of the electro-active material in the fabricated electrode (g), and υ is the potential scan rate (V s^{-1}).

In addition, Fig. 5B shows a relation between C_s values and the scan rate. The general trend is that C_s values are inversely proportional to the scan rate. As mentioned earlier, it is possible for ions to access the electrode surface easily at low scan rates, which can substantially improve electrosorption capacitance. In the case of the 5 wt.% CeO$_2$@AC electrode material, its C_s values were higher than both pristine AC and 10 wt.% CeO$_2$@AC. At a scan rate of 10 mV s^{-1}, the evaluated C_s of 5 wt.% CeO$_2$@AC was 262 Fg^{-1}, which exceeded that of pristine AC (163.8 Fg^{-1}) and 10 wt.% CeO$_2$@AC (209 Fg^{-1}).

These results indicate that the 5 wt.% CeO$_2$@AC composite electrode material outperformed the alternative materials in terms of EDL capacitance behavior toward salt ion electrosorption, thus improving the charge transfer and contact area [22]. EIS measurements can be employed as an instrument to identify the suitability of electrode materials regarding various factors, including the electrolyte solution and the electrode material charge transfer behavior at the interface between the electrode and electrolyte.

The Nyquist plots of AC and 5 wt.% CeO$_2$@AC in 1 M NaCl for the frequency range of 0.01–10 Hz, along with an AC perturbation of 5 mV, are shown in Fig. 6. In most cases for electrode materials, a visible semicircle should be detectable in the high-frequency region. The semicircle is linked closely to factors such as the electron transfer process, the electrode's electrical conductivity, and the solution interface.
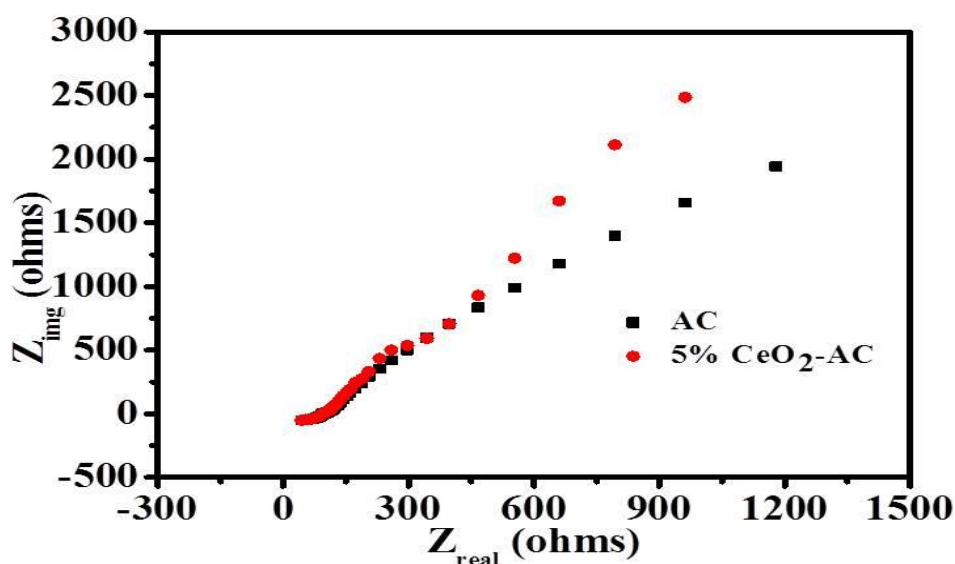
Figure 6. Nyquist plots of AC and 5 wt.% CeO$_2$@AC in 1.0 M NaCl solution with a frequency range of 10 kHz–100 mHz, amplitude of 5 mV, and potential value of 0 mV.

As Fig. 6 indicates, every electrode exhibited an inclined line in the high-frequency section alternate of semicircle shape, which indicates a substantial fall in polarization resistance [44-46].

Additionally, in the low-frequency section, the continuous nature of the vertical line was observed, which is attributable to their characteristic double-layered capacitive behavior. This is suggestive of the considerable capacitive behavior of the electrode materials, and it indicates the rapid diffusion of ions into the material's pores [46, 47].

The primary variables that influence the commercial potential of CDI electrodes are cost and service lifetime. Therefore, the regeneration capability of AC and 5 wt.% CeO_2@AC was studied at 1, 1.2, and 1.4 V in 1 M NaCl aqueous solution via the charge-discharge test (Fig. 7A). At both electrodes, the plots displayed high electrochemical stability and good reversibility. In the course of the desorption process, the conductivity values moved back to their start values, which indicates the full desorption of the adsorbed ions to the electrolyte following voltage release. Significantly, these results suggest the positive regeneration performance of the materials. Compared to pristine AC, the time during the discharge process was longer for 5 wt.% CeO_2@AC. The results after testing the cycling stability of 5 wt.% CeO_2@AC were high, where the test was run for 20 cycles at 1.4 V in 1 M NaCl aqueous solution.
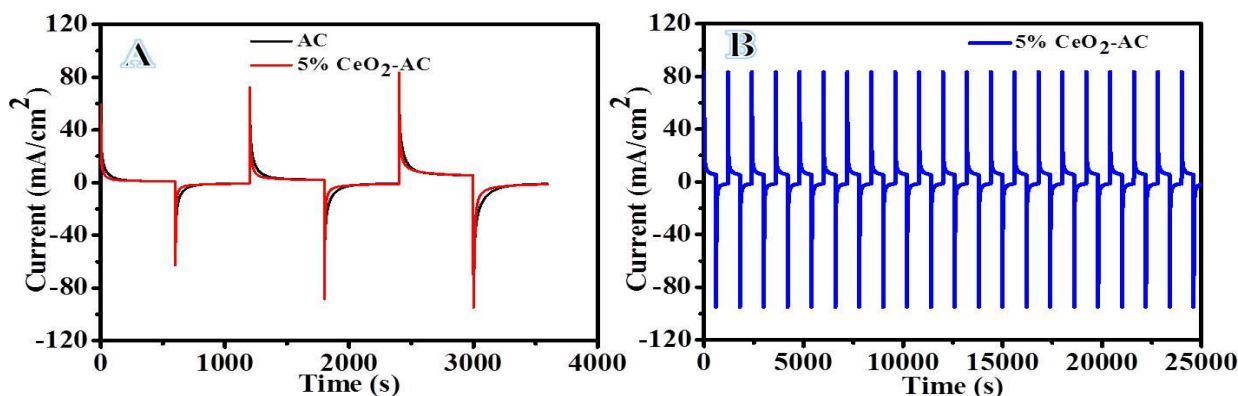
Figure 7. PCD of AC and 5 wt.% CeO_2@AC in 1.0 M NaCl solution at 1, 1.2, and 1.4 V (A). Desalination retention study by repeated cyclization of 5 wt.% CeO_2@AC for 20 cycles (B).

Using a potential window ranging from −0.4 to 0.6 V and current densities ranging from 1 A g^{-1} to 9 Ag^{-1}, the GCD test was undertaken for 5 wt.% CeO_2@AC, as shown in Fig. 8A. For all current densities, triangle-shaped profiles were observed; at the same time, the discharged time was inversely proportional to current density, indicating high capacitance behavior and electrochemical reversibility. The long-term stability of 5 wt.% CeO_2@AC was maintained after 20 cycles of GCD at 5 A/g (Fig. 8B). Therefore, given that a similar pattern was obtained after 20 cycles, this serves as a confirmation of electrochemical reversibility and stability. These results concerning the high electrochemical cycling stability of 5 wt.% CeO_2@AC as a composite electrode material indicate that it represents an excellent candidate for CDI systems.
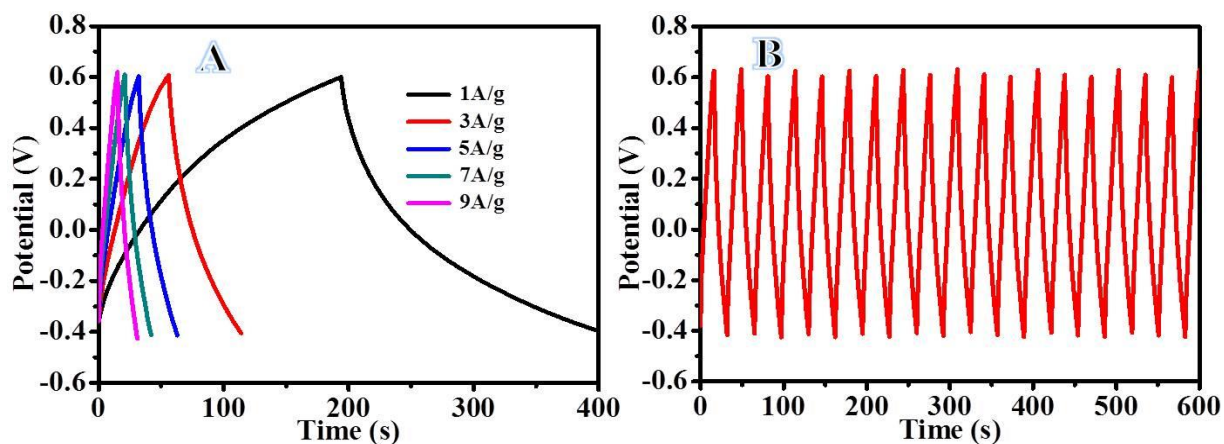
Figure 8. GCD profiles for 5 wt.% CeO$_2$@AC in 1.0 M NaCl solution at current densities of 1, 3, 5, 7, and 9 A g^{-1} (A). Stability test using charge-discharge alternative mode for 20 cycles at potential values from -0.4 to 0.6 V (B).

3.3 CDI cell performance

Fig. 9A shows the CDI cell's electrosorption performance with three electrode materials: AC, 5 wt.% CeO$_2$@AC, and 10 wt.% CeO$_2$@AC.

Figure 9. Electroadsorption performance for pristine AC, 5 wt% CeO$_2$@AC, and 10 wt% CeO$_2$@AC in **NaCl** (100 µS cm^{-1}) at 1.4 V (A). Effect of different potentials on CDI performance with 5 wt% CeO$_2$@AC (B). Electrosorption capacity at different applied potentials (C).

These results were achieved with NaCl aqueous solution (100 μS cm^{-1}) at a flow rate of 10 ml min^{-1} and a potential between the electrodes of 1.4 V. After applying the potential between the CDI electrodes, a rapid decrease occurred in the saline solution's initial conductivity. This is due to the fact that the NaCl ions were adsorbed by the charged electrodes. The electrosorption process tapered off until the saturation of the surface of the electrode with salt ions, after which electrosorption equilibrium was reached. The adsorption capacity of 5 wt.% CeO$_2$@AC was higher than AC and 10 wt.% CeO$_2$@AC. Additionally, the CDI performance of 5 wt.% CeO$_2$@AC was tested at different applied potentials (namely, 1, 1.2, and 1.4 V, as shown in Fig. 9B), again using 100 μS cm^{-1} NaCl solution. The conductivity of the saline solution decreased with the increase in voltage. At the same time, the electrosorption capacity of 5 wt.% CeO$_2$@AC increased (5.8, 7.8, and 8.9 mg g^{-1}) with an increase in applied voltage (1, 1.2, and 1.4 V) at 100 μS cm^{-1} NaCl solution (Fig. 9C).

As an electrode material, this study indicates that 5 wt.% CeO$_2$@AC has a favorable electrosorption capacity compared to other metal oxides doped carbon materials reported in previous literature (Table 1). The electrosorption capacity may be attributable to the way the incorporation of CeO$_2$ NPs to AC lowered the internal resistance and improved the electrical conductivity and electrochemical behavior of the electrode material, thereby resulting in higher ion transport toward the electrodes. In view of this, a substantial rise occurred in the salt-ion adsorption capacity.

Table 1. Electrosorption capacity of different metal oxides doped carbon materials

Materials	Initial salt concentration (mg L^{-1})	Electrosorption capacity (mg g^{-1})	Applied voltage (V)	Ref.
Aerographene/TiO2	250	1.2	9.9	[48]
MnO$_2$/CNT-CS	58.4	6.01	1.0	[49]
CeO$_2$@GNFs	48	7.2	1.4	[11]
Mn oxide -AC	600	8.86	1.2	[50]
NiMn Oxide-AC	600	7.25	1.2	[50]
CeO$_2$@AC	100	8.9	1.4	This work

4. CONCLUSION

In this study, varying compositions of CeO$_2$@AC were fabricated via a hydrothermal treatment process in aqueous alkaline media. The experimental results indicate that at a scan rate of 10 mV s^{-1}, the specific capacitance of 5 wt.% CeO$_2$@AC (262 Fg^{-1}) exceeded that of pristine AC (163.8 Fg^{-1}) and 10 wt.% CeO$_2$@AC. The long-term stability of 5 wt.% CeO$_2$@AC was also high after 20 cycles of GCD at 5 A/g, and the material's electrosorption capacity increased with an increase in applied voltage in 100 μS cm^{-1} NaCl solution (namely, achieving 5.8, 7.8, and 8.9 mg g^{-1} at 1, 1.2, and 1.4 V, respectively).

References

1. Z.Y. Yang, L.J. Jin, G.Q. Lu, Q.Q. Xiao, Y.X. Zhang, L. Jing, X.X. Zhang, Y.M. Yan, and K.N. Sun, *Adv. Funct. Mater.*, 24 (2014) 3917.
2. H. Li, L. Zou, L. Pan,and Z. Sun, *Environ. Sci. Technol.*, 44 (2010) 8692.
3. T. Humplik, J. Lee, S. O'hern, B. Fellman, M. Baig, S. Hassan, M. Atieh, F. Rahman, T. Laoui, and R. Karnik, *J. Nanotechol.*, 22 (2011) 292001.
4. F.A. AlMarzooqi, A.A. Al Ghaferi, I. Saadat, and N. Hilal, *Desalination*, 342 (2014) 3.
5. K. Rambabu, G. Bharath, A. Hai, S. Luo, K. Liao, M.A. Haija, F. Banat, and M. Naushad, *J. Cleaner Prod.*, 272 (2020) 122626.
6. A. Yousef, R.A. Hameed, S.F. Shaikh, A. Abutaleb, M. El-Halwany, and A.M. Al-Enizi, *Sep. Sci. Technol.,* 254 (2021) 117602.
7. P.-A. Chen, H.-C. Cheng, and H.P. Wang, *J. Cleaner Prod.*, 174 (2018) 927.
8. H. Duan, T. Yan, Z. An, J. Zhang, L. Shi, and D. Zhang, *RSC Adv.,* 7 (2017) 39372.
9. S. Zhao, T. Yan, Z. Wang, J. Zhang, L. Shi, and D. Zhang, *RSC Adv.,* 7 (2017) 4297.
10. A.M. Al-Enizi, R.A. Hameed, M. El-Halwany, M. Bakrey, S.F. Shaikh, and A. Yousef, I. Science, *J. Colloid Interface Sci.,* 581 (2021) 112.
11. A. Yousef, A.M. Al-Enizi, I.M. Mohamed, M. El-Halwany, M. Ubaidullah, and R. Brooks, *Ceram. Int.,* 46 (2020) 15034.
12. T. Hussain, Y. Wang, Z. Xiong, J. Yang, Z. Xie, and J. Liu, *J. Colloid Interface Sci.*, 532 (2018) 343.
13. H. Sakar, I. Celik, C. Balcik-Canbolat, B. Keskinler, and A. Karagunduz, *Energy Environ. Sci.*, 215 (2019) 1415-1423.
14. M.E. Suss, T.F. Baumann, W.L. Bourcier, C.M. Spadaccini, K.A. Rose, J.G. Santiago, and M. Stadermann, *Chem. Eng. J.*, 5 (2012) 9511.
15. C.-C. Huang, and J. He, *Carbon*, 221 (2013) 469.
16. R.L. Zornitta, F.J. García-Mateos, J.J. Lado, J. Rodríguez-Mirasol, T. Cordero, P. Hammer, and L.A. Ruotolo, *Carbon*, 123 (2017) 318.
17. C. Kim, P. Srimuk, J. Lee, S. Fleischmann, M. Aslan, and V. Presser, *Carbon,* 122 (2017) 329.
18. Q. Dong, G. Wang, T. Wu, S. Peng, and J. Qiu, *J. Colloid Interface Sci.*, 446 (2015) 373.
19. Q. Dong, G. Wang, B. Qian, C. Hu, Y. Wang, and J. Qiu, *Electrochim. Acta*,137 (2014) 388.
20. N. Zouli, R.A. Hameed, A. Abutaleb, M. El-Halwany, M.H. El-Newehy, and A. Yousef, *J. Mater. Res. Technol.*, 15 (2021) 3795.
21. S. Rezma, I.B. Assaker, R. Chtourou, A. Hafiane, and H. Deleuze, *Mater. Res. Bull.*, 111 (2019) 222.
22. A.S. Yasin, M. Obaid, I.M. Mohamed, A. Yousef, and N.A.M Barakat, *RSC Adv.*, 7 (2017) 4616.
23. Y. Liu, C. Nie, X. Liu, X. Xu, Z. Sun, and L. Pan, *RSC Adv.*, 5 (2015) 15205.
24. J. Yang, L. Zou, H. Song, and Z. Hao, *Desalination*, 276 (2011) 199.
25. J.J. Wouters, M.I. Tejedor-Tejedor, J.J. Lado, R. Perez-Roa, and M.A. Anderson, *Desalination*, 165 (2018) E148.
26. T. Yumak, D. Bragg, and E.M Sabolsky, *Appl. Surf. Sci.*, 469 (2019) 983.
27. A. Corma, P. Atienzar, H. Garcia, and J.-Y. Chane-Ching, *Nature materials*, 3(6) (2004) 394.
28. Q. Su, L. Chang, J. Zhang, G. Du, and B. Xu, *The Journal of Physical chemistry* C, 117 (2013) 4292.
29. X. Zhao, Y. Du, W. Ye, D. Lu, X. Xia, and C. Wang, *New J. Chem.*, 37 (2013) 4045.
30. A. Trovarelli, *Catalysis Reviews*, 38 (1996) 439.
31. T. Li and H. Liu, *Powder Technol.*, 327 (2018) 275.
32. Z. Ji, X. Shen, H. Zhou, and K. Chen, *Ceram. Int.*, 41 (2015) 8710.
33. L. Aravinda, K.U. Bhat, and B.R. Bhat, *Mater. Lett.*, 112 (2013) 158.
34. D.M. El-Gendy, R.A. Hameed, A.M. Al-Enizi, M. Bakrey, M. Ubaidullah, and A. Yousef, *Ceram.*

Int., 46 (2020) 27437.

35. J. Shu, S. Cheng, H. Xia, L. Zhang, J. Peng, C. Li, and S. Zhang, *RSC Adv*., 7 (2017) 14395.
36. R. Murugan, G. Vijayaprasath, T. Mahalingam, and G. Ravi, *Appl. Surf. Sci*., 390 (2016) 583.
37. L. Li, L. Zou, H. Song, and G. Morris, *Carbon*, 47 (2009) 775.
38. C.-T. Hsieh and H. Teng, *Carbon*, 40 (2002) 667.
39. H. Li, S. Liang, J. Li, and L. He, *J. Mater. Chem*. A, 1 (2013) 6335.
40. B.H. Park and J.H. Choi, *Electrochim. Acta*, 55 (2010) 2888.
41. Z.L. Wang, X. Kong, and J. Zuo, *Phys. Rev. Lett*., 91 (2003) 185502.
42. J. Ma, Y. Cheng, L. Wang, X. Dai, and F. Yu, *Chem. Eng. J.,* 384 (2020) 123329.
43. F. Xing, T. Li, J. Li, H. Zhu, N. Wang, X. Cao, *CNano Energy*, 31 (2017) 590.
44. A.K. Mishra and S. Ramaprabhu, *The Journal of Physical Chemistry* C, 115 (2011) 14006.
45. M.D. Stoller, S. Park, Y. Zhu, J. An, and R.S. Ruoff, *Nano letters*, 8(2008) 3498.
46. M.R. Vengatesan, I.F.F. Darawsheh, B. Govindan, E. Alhseinat, and F. Banat, *Electrochim. Acta*, 297 (2019) 1052.
47. L. Chang, J. Li, X. Duan, and W. Liu, *Electrochim. Acta*, 176 (2015) 956.
48. H. Yin, S. Zhao, J. Wan, H. Tang, L. Chang, L. He, H. Zhao, Y. Gao, and Z. Tang, *Adv. Mater*., 25 (2013) 6270.
49. Y.H. Liu, T.C. Yu, Y.W. Chen, and C.H. Hou, *ACS Sustainable Chem. Eng*., 6 (2017) 3196.
50. A.T. Angeles, J. Park, K. Ham, S. Bong, and J. Lee, *Sep. Purif. Technol*., 280 (2021) 119873